ELSEVIER

Intermetallics 8 (2000) 953–962

Intermetallics

www.elsevier.com/locate/intermet

Thermodynamic reassessment of the Mo–Si and Al–Mo–Si systems

Y. Liu [a,b], G. Shao [a,*], P. Tsakiropoulos [a]

[a] *School of Mechanical and Materials Engineering, University of Surrey, Guildford, Surrey GU2 7XH, UK*
[b] *General Research Institute for Non-ferrous Metals, Beijing, 100088, PR China*

Received 11 May 2000; accepted 19 May 2000

Abstract

The thermodynamic properties and phase diagrams of the Mo–Si and Al–Mo–Si systems are assessed, and a complete thermodynamic description is obtained. The calculation results show good agreement with the experimental data. The high temperature phase equilibria involving the C40 and $C11_b$ $MoSi_2$ structures in the Mo–Si binary and Al–Mo–Si ternary systems have been clarified.

Keywords: A. Silicides, various; A. Ternary alloy systems; B. Phase diagram; B. Thermodynamic and thermochemical properties; E. Phase diagram prediction

1. Introduction

The need for materials for high temperature ($T > 1773$ K) applications has led to the development of materials based on molybdenum disilicide in view of its favorable properties, which include high melting point (2293 K [1]), excellent oxidation resistance at high temperatures and reasonable density (6.24 g/cm^3 [2]). However, this compound suffers from pest oxidation at low temperatures and poor ductility and toughness at room temperature. Current investigations of high-temperature $MoSi_2$-based intermetallic matrix composites are directed towards the development of multiphase microstructures with enhanced mechanical properties while maintaining the superior oxidation resistance of $MoSi_2$. It has been reported that adding aluminum, which can stabilize the C40 structure, can impart a 'metallic character' to the molybdenum disilicide and improve its ductility. It has also been shown that aluminum addition can be used to improve the oxidation resistance of $MoSi_2$ by producing Al_2O_3 via an in-situ displacement reaction [3,4]. Thus, the mechanical properties as well as oxidation resistance of $MoSi_2$ can be improved by alloying with aluminum [5–7]. However, there are conflicting reports that indicate that the addition of aluminum to $MoSi_2$ actually decreases its oxidation resistance under both cyclic and static conditions [8,9].

Despite the technological importance of $MoSi_2$ and $Mo(Si,Al)_2$, the thermodynamics of the Al–Mo–Si ternary system as well as the high-temperature phase equilibria in the vicinity of $MoSi_2$ in the Mo–Si binary system are still incomplete. In order to clarify the effect of the addition of aluminum to $MoSi_2$, the phase equilibria in the Mo–Si and Al–Mo–Si systems need to be established.

Of the three constitutional binary systems of the Al–Mo–Si ternary system, the available assessments of the Al–Mo [10] and Al–Si [11] systems are considered satisfactory. The calculated phase diagrams of the Al–Mo and Al–Si systems are presented in Figs. 1 and 2, respectively. However, the available assessment of the Mo–Si system still needs improvement.

An extensive review of available experimental work on the Mo–Si system has been performed by Gokhale and Abbaschien [1]. This system has been assessed using the CALPHAD method by several authors [12–16], but their results differ considerably, and show remarkable disagreement with experimental data. Also, the Mo–Si system has been a subject of recent debate concerning the high-temperature phase equilibria in the vicinity of $MoSi_2$.

Svechnikov et al. [17–19] reported that the $MoSi_2$ phase undergoes a polymorphic transformation from a low-temperature tetragonal $C11_b$ structure to a high-temperature hexagonal C40 structure at about 2173 K.

* Corresponding author. Tel.: +44-01483-876288; fax: +44-01483-259508.
E-mail address: g.shao@surrey.ac.uk (G. Shao).

0966-9795/00/$ - see front matter
PII: S0966-9795(00)00068-6

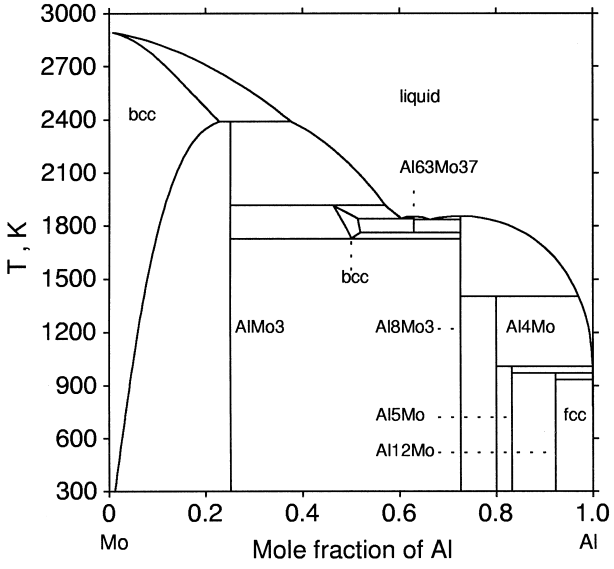

Fig. 1. The Al–Mo binary phase diagram calculated from the thermodynamic description by Saunders [10].

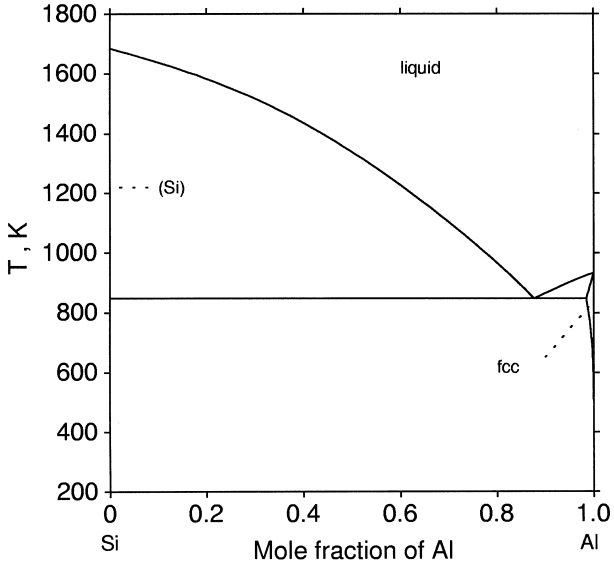

Fig. 2. The Al–Si binary phase diagram calculated from the thermodynamic description by Chakraborti and Lukas [11].

The hexagonal C40 $MoSi_2$ was observed in Mo–Si thin films and plasma spray processed samples, but there was no direct evidence in support of the polymorphic transformation of $MoSi_2$ [1,20,21]. Frankwicz et al. [20] measured the phase equilibria data in the $MoSi_2$–$TiSi_2$ quasi-binary system using X-ray diffraction and electron microscopy. The experimental results showed that the hexagonal $(Ti,Mo)Si_2$-C40 phase formed via a peritectic reaction between liquid and $MoSi_2$-$C11_b$. The primary dendritic structure during solidification in $(Ti_{1-x}Mo_x)Si_2$, where $x \geqslant 0.80$, was determined to be tetragonal $MoSi_2$-$C11_b$. The $C11_b$ structure existed up to the melting point in the Mo–Si binary system. This was supported by Boettinger et al. [22], who presented the phase equilibria data on the $MoSi_2$–$TiSi_2$ and $MoSi_2$–$TaSi_2$ quasi-binary systems, and pointed out that it was impossible for the $C11_b$ to C40 polymorphic transformation to occur in pure $MoSi_2$. Boettinger et al. [22] demonstrated that $MoSi_2$ retains the $C11_b$ structure up to the melting point and that the C40 structure reported in other studies was caused by contamination. More recently, Frankwicz et al. [21] investigated the phase equilibrium of $MoSi_2$ in the Mo–Si system in arc-melted and plasma-sprayed samples. The analysis of solidification microstructures and X-ray diffraction patterns of arc-melted $MoSi_2$-based alloys indicated that solidification took place by the formation of primary $MoSi_2$-$C11_b$. Retained $MoSi_2$-C40 phase in plasma sprayed samples exhibited an irreversible transformation to $MoSi_2$-$C11_b$ at $T \approx 1110$ K. The authors pointed out that the metastable melting point of $MoSi_2$-C40 was 2299 K. In-situ high temperature X-ray diffraction pattern from an annealed (1800s) $Mo_{0.45}Si_{0.55}$ sample at 2150 K (lower than the melting point of $MoSi_2$ 2293 K [1] and the proposed C40 to C11b polymorphic transformation temperature 2173 K [17–19]) showed the characteristic $MoSi_2$-$C11_b$ X-ray diffraction peaks. It should be pointed out that direct evidence is still needed in order to clarify the high-temperature phase equilibria in the Mo–Si binary system.

There is limited experimental data on the Al–Mo–Si ternary system, and the currently available isothermal sections are inconsistent with each other. Fig. 3a shows the 1873 K isothermal section for the Al–Mo–Si system proposed by [23]. According to [23], there are two ternary compounds, C40 and C54, in this system. It should be noted that this diagram is not in agreement with the presently accepted Al–Mo binary phase diagram [10] since it presented Al_2Mo as a stable phase, and showed the absence of any liquid phase at 1873 K. This isothermal section of [23] was not truly an isothermal, either, as the data spans a temperature range from 1873 K on the Mo–Si side to 1623 K on the Al-rich portion of the ternary diagram. This isothermal section was modified by Guzei [24] with certain corrections which became necessary in order to consider the noticeable regions of the homogeneity of the binary phases Mo_5Si_3 and Mo_3Al, and the fact that the Al_2Mo phase has the composition $Al_{63}Mo_{37}$ according to [25].

More recent isothermal sections of the Al–Mo–Si system were established at 1823 K [6] (Fig. 3b) and 1323 K [26] (Fig. 3c). In both diagrams the C54 phase was not present and the Al-rich side of the $Mo(Si,Al)_2$ composition ended at the Al_8Mo_3 phase, which is present in the currently accepted Al–Mo binary phase diagram [10]. These diagrams agree on the relative placement of the C40, $C11_b$ and Mo_5Si_3 phases but differ with respect to their ranges of solubility. Costa e Silva [15] produced the isothermal sections of the Al–Mo–Si system at 1273

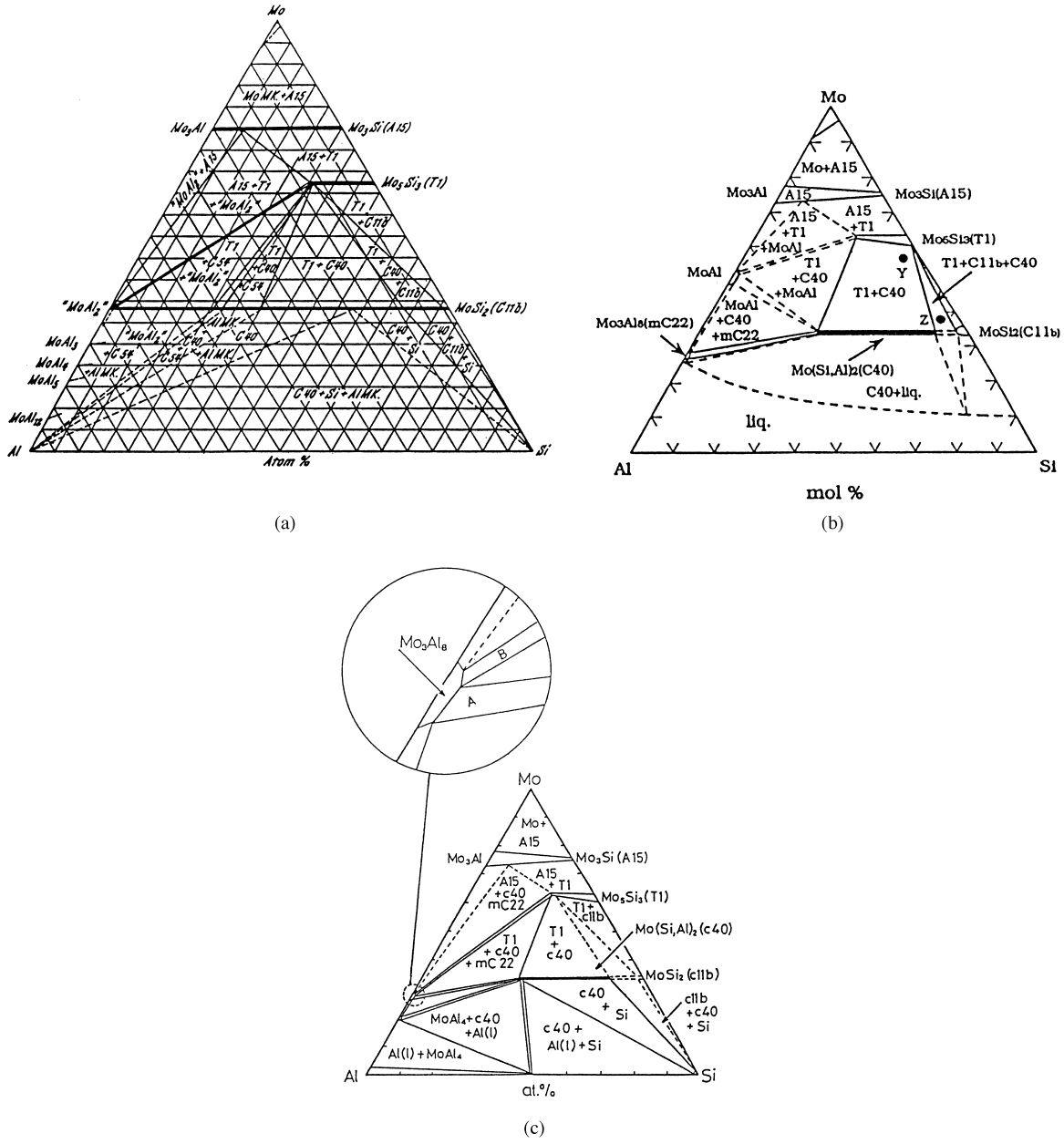

Fig. 3. (a) The 1873 K isothermal section of the Al–Mo–Si ternary system proposed by Brukl et al. [23]; (b) the 1823 K isothermal section of the Al–Mo–Si ternary system proposed by Yanagihara et al. [6]; (c) the 1323 K isothermal section of the Al–Mo–Si ternary system proposed by Maruyama et al. [26].

K and 1673 K. The experimental results revealed the existence of the C54 phase, at least at 1673 K. Eason et al. [27] measured the isothermal section of this ternary system at 1673 K. Their results also showed the presence of the C54 phase.

The Al–Mo–Si system was thermodynamically assessed by Costa e Silva [15]. However, in their thermodynamic assessment, they did not consider the C54 phase. Furthermore, the constitutional binary systems Al–Mo and Mo–Si that they used to describe the properties of the Al–Mo–Si ternary system were greatly different from the currently accepted phase diagrams. Therefore, critical thermodynamic assessments of both the Mo–Si and Al–Mo–Si systems are needed.

In this paper, the dendrite morphology on the free surface of as cast $MoSi_2$ ingot has been studied in order to record the history of phase equilibria during solidification. The Mo–Si binary and Al–Mo–Si ternary systems are reassessed using the CALPHAD method. The thermodynamic properties of Al–Mo and Al–Si systems are taken from the assessments of Saunders [10] and Chakraborti [11], respectively.

2. Free surface dendrite morphology of $MoSi_2$ ingot

A $MoSi_2$ ingot about 350 g in weight was produced by arc-melting high purity materials. The sample was remelted several times to ensure homogenity. The free surface of the sample was studied using scanning electron microscopy. Fig. 4 shows the representative dendrite morphology, typical of a tetragonal primary phase, instead of a hexagonal structure. Therefore, the absence of the $C11_b$ to C40 polymorphic transformation proposed by [20–22] is directly confirmed.

3. Thermodynamic model

There are basically two types of phases in the Al–Mo–Si system, solution phases and intermetallic compounds. The stable solution phases present in the Al–Mo–Si system are liquid, bcc (Mo), fcc (Al) and diamond (Si). There are seven stable intermetallic compounds in the Al–Mo system, Mo_3Al, AlMo, $Al_{63}Mo_{37}$, Al_8Mo_3, Al_4Mo, Al_5Mo and $Al_{12}Mo$, which were modeled as stoichiometric compounds by Saunders [10]. No stable intermetallic compound exists in the Al–Si system [11]. In the Mo–Si system, there are three stable intermetallic compounds Mo_3Si, Mo_5Si_3 and $MoSi_2$-$C11_b$. Two ternary compounds of the C40 and C54 structures exist in the Al–Mo–Si system. These phases are all modeled using the sublattice model [28]. The Gibbs energy of the sublattice model is expressed as:

$$G_m = G_m^{ref} + G_m^{id} + {}^{ex}G_m \quad (1)$$

The term G_m^{ref} defines the Gibbs energy reference surface and is associated with the complete occupation of each sublattice by one component mixing on it,

$$G_m^{ref} = \sum_I P_I(Y)\cdot {}^0G_I \quad (2)$$

where I denotes a component array, which defines one component for each sublattice. Y is the component matrix. $P_I(Y)$ represents the corresponding product of the site fractions from the Y matrix. ${}^0G_I$ represents the Gibbs energy of the compound defined by I.

The term G_m^{id} expresses the Gibbs energy arising from ideal entropy of mixing of the component on each separate sublattice,

$$G_m^{id} = RT\sum_s a^s \sum_i y_i^s \ln y_i^s \quad (3)$$

where a^s is the number of sites on the sublattice s per mole of formula units of the phase, and y_i^s represents the site fraction of component i on sublattice s.

The term ${}^{ex}G_m$, the excess Gibbs energy, represents the interaction energies between different components in the same sublattice,

$${}^{ex}G_m = \sum_{Z>0}\sum_{IZ} P_{IZ}(Y)\cdot L_{IZ} \quad (4)$$

where IZ refers to a component array of the Zth order, e.g. $I1$ refers to a component array of the first order, where one sublattice contains two components, but the remaining sublattices are occupied by only one component. L_{IZ} is the interaction parameter. A detailed review of the sublattice model can be found in [29].

According to the orientation, shape and solubility range of the compound phases in the Al–Mo–Si system, compound phases whose ternary solubility is considered are listed in Table 1. It should be pointed out that the sublattice model with mixing occurring on only one sublattice is identical to the substitutional solution model. In this work, a single sublattice is assigned to the liquid and diamond phases. For the bcc and fcc solution phases, an additional site for the virtual vacancy is assigned (Table 1). In this case, the Gibbs energy can be simplified as:

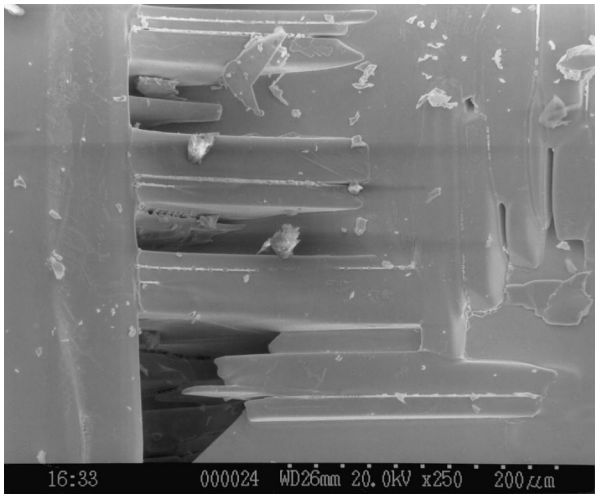

Fig. 4. Secondary electron image of the free surface dendrite morphology of the as cast $MoSi_2$ ingot.

Table 1
Summary of the models adopted[a]

Phase	Model
Liquid	(Al, Mo, Si)
bcc	(Al, Mo, Si)$(Va)_3$
fcc	(Al, Mo, Si)(Va)
Diamond	(Si, Al)
Mo_3(Al, Si)	$(Mo)_{0.75}$(Si, Al)$_{0.25}$
Mo_5Si_3	(Mo, Si)$_{0.625}$(Si, Mo, Al)$_{0.375}$
$MoSi_2$_$C11_b$	$(Mo)_{0.333}$(Si, Al)$_{0.667}$
C40	$(Mo)_{0.333}$(Si, Al)$_{0.667}$
C54	$(Mo)_{0.333}(Si)_{0.233}(Al)_{0.434}$

[a] Predominant atom, if any, in each sublattice is underlined.

$$G_m = \sum_i x_i {}^0G_i + RT\sum_i x_i \ln x_i + {}^{ex}G_m \quad (5)$$

where x_i refers to the mole fraction of component i (i=Al, Mo, Si). ${}^0G_i$ is the molar Gibbs energy of pure component i. ${}^{ex}G_m$ is expressed in Redlich–Kister polynomials [30],

$$\begin{aligned} {}^{ex}G_m = {} & x_{Al}x_{Mo}\sum_m {}^mL_{Al,Mo}(x_{Al}-x_{Mo})^m + \\ & x_{Al}x_{Si}\sum_m {}^mL_{Al,Si}(x_{Al}-x_{Si})^m \\ & x_{Mo}x_{Si}\sum_m {}^mL_{Mo,Si}(x_{Mo}-x_{Si})^m + \\ & x_{Al}x_{Mo}x_{Si}L_{Al,Mo,Si} \end{aligned} \quad (6)$$

where ${}^mL_{i,j}$ and $L_{Al,Mo,Si}$ are the binary and ternary interaction parameters, respectively.

4. Evaluation of the thermodynamic parameters

The model parameters are evaluated using the Parrot module in the Thermo-Calc program package [31]. This program is able to take various kinds of experimental data in the operation. It works by minimizing an error sum with each kind of the selected data values, given a certain weight. The weight is chosen and adjusted based on the data uncertainties given in the original publications, until most of the selected experimental information is reproduced within the expected uncertainty limits. All thermodynamic calculations are carried out using the Thermo-Calc program package.

4.1. The Mo–Si binary system

The phase diagram data summarized by [1,13] are used as a guide for selecting the experimental phase diagram data. The critical assessments by [3,12,14] are used as a guide for selecting the initial values of interaction parameters. The thermodynamic description of the liquid phase is developed first, by fitting the mixing enthalpies of liquid phase [32]. Then, keeping these parameters fixed, the parameters of bcc, Mo_3Si, Mo_5Si_3 and $MoSi_2$-$C11_b$ are fitted separately based on the phase diagram data and thermodynamic data. Finally, all parameters are optimized simultaneously by using all of the selected experimental data.

4.2. The Al–Mo–Si ternary system

The ternary interaction parameters in the liquid, bcc, fcc and diamond phases are not considered in this work because of the lack of experimental data on the solution phases. The initial Gibbs energy values of the hypothetical compounds $MoAl_2$-$C11_b$, $MoAl_2$-C40, Mo_5Al_3-$D8_m$ are taken from Miedema's estimated heats of formation [33]. The initial Gibbs energy value of $MoSi_2$–C40 is based on the total energy difference of $MoSi_2$ in the $C11_b$ and C40 crystal structures at 0 K, which is calculated by Carlsson [34] and Meschter [35] using *ab-inito* self-consistent band structure theory. All the available phase diagram data is used to optimize the interaction parameters.

5. Results and discussion

By means of the computerised optimisation, a complete and self-consistent thermodynamic description for the Mo–Si binary and Al–Mo–Si ternary systems is obtained and listed in the Appendix. The reference state of the Gibbs energy of individual phases is the so-called standard element reference, that is, the enthalpies of the pure elements in their stable state at 298.15 K.

5.1. The Mo–Si binary system

The calculated and measured enthalpies of mixing in the liquid phase at 3087 K are presented in Fig. 5. The results of [12,14,15] are also shown in Fig. 5. It can be seen that the calculated values of [12] differ greatly with the experimental data [32]. The calculated values of [14] agree well with the experimental values except near the range of $x_{Si}=0.4$. The calculated results of this work and [15] agree well with the experimental ones.

The calculated enthalpies of formation and entropy of formation of intermediate compounds at 298 K are listed in Tables 2 and 3, respectively. All available literature values (experimental and assessed) are listed in these tables. It can be seen that the enthalpies of formation and entropy of formation calculated in the present work agree well with the experimental values. The entropy of formation of Mo_5Si_3 and $MoSi_2$ given by [14–16] differs

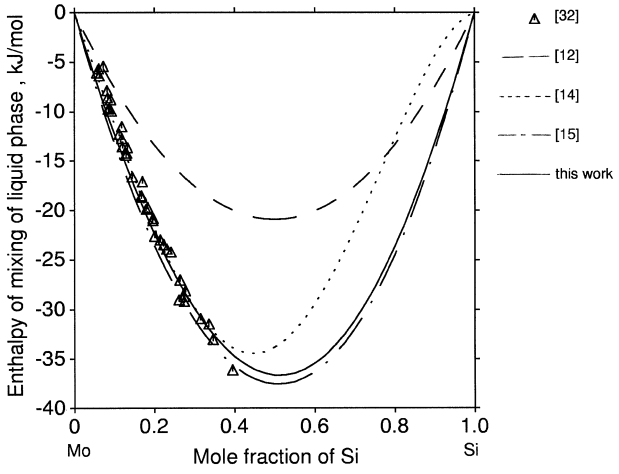

Fig. 5. Comparison between the calculated and measured enthalpy of mixing of the liquid phase of the Mo–Si system at 3087 K.

Table 2
Enthalpies of formation of intermetallic phases in the Mo–Si system at 298 K

Phase	x_{Si}	ΔH_f (kJ/mole of atoms)								
		Experimental value				Assessed value				
		[36]	[37]	[38]	[39]	[12]	[14]	[15]	[16]	This work
Mo_3Si	0.25	−24.89±2.09	−29.1±3	−29.1±3	−25.418	−28.372	−29.7102	−31.750	−29.8052	−27.900
Mo_5Si_3	0.375	−38.62±2.09[a]	−38.7±3	−38.7±3	−37.813	−38.682	−37.0084	−39.1725	−37.0884	−38.980
$MoSi_2$	0.667	−43.76±2.09	−43.9±3	−43.9±3	−39.609	−42.530	−46.5157	−45.6667	−46.5157	−45.156

[a] $T = 2000$ K.

Table 3
Entropy of formation of intermetallic phases in the Mo–Si system at 298 K

Phase	x_{Si}	$\Delta S_{f,}$ [J/(K mole of atoms)]								
		Experimental value				Assessed value				
		[36]	[37]	[38]	[39]	[12]	[14]	[15]	[16]	This work
Mo_3Si	0.25	0.130±0.293	0.42±1.3	0.42±1.2	0.4184	0.296	0.5096	2.5	0.6177	0.28
Mo_5Si_3	0.375	−0.794±1.254[a]	1.0±1.3	1.0±1.2	0.9894	0.54	3.78675	5.745	3.8197	1.349
$MoSi_2$	0.667	−2.625±4.222	−0.42±1.3	−0.4±1.2	−0.406	−0.07	2.83236	4.2533	2.8423	−0.223

[a] $T = 2000$ K.

greatly from the available experimental data. The entropy of formation of Mo_3Si given by [15] also differs greatly from the available experimental data [36–39]. Chart [38] pointed out that the entropy of fusion of transition metal silicides versus their melting points obeys the similar trends to those shown by the pure elements [40], that is there is a correlation between the entropy of fusion and melting point within a group of elements that have a particular crystal structure. The enthalpies of fusion and the melting points reflect the cohesion energy. The relationships between enthalpies of fusion and entropy of fusion of different silicides vs. melting points are shown in Figs. 6 and 7, respectively. Our calculated enthalpies of fusion and entropy of fusion of $MoSi_2$ and Mo_5Si_3 agree well with the general trends.

The calculated phase diagram of the Mo–Si system is compared with various experimental phase boundary data in Fig. 8. Table 4 presents the comparison of the calculated invariant equilibria with the literature values. It can be seen that the calculation agrees well with the experimental data.

5.2. The Al–Mo–Si ternary system

The calculated isothermal sections at 1273, 1673, 1823 and 1873 K are shown in Figs. 9–12, respectively. The available experimental data is also shown in these figures. It can be seen that both the calculated phase boundary and the direction of tie lines agree well with most of the available values in literature. It should be pointed out that

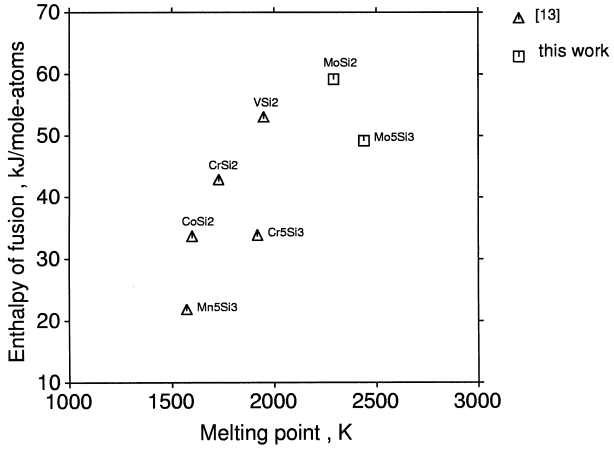

Fig. 6. The relationship between enthalpy of fusion and the melting point of different silicides.

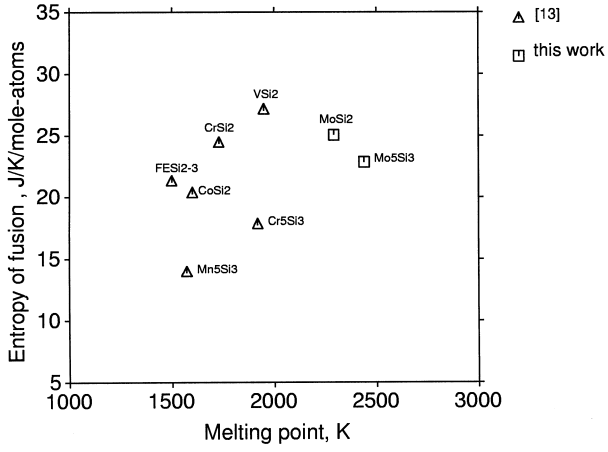

Fig. 7. The relationship between entropy of fusion and the melting point of different silicides.

the phase boundary of $Mo_3(Si,Al)$ differs slightly from values in literature because the homogeneity range of Mo_3Al in the binary Al–Mo is not considered [10]. The phase boundary between $MoSi_2$-$C11_b$, C40 and Mo_5Si_3 at

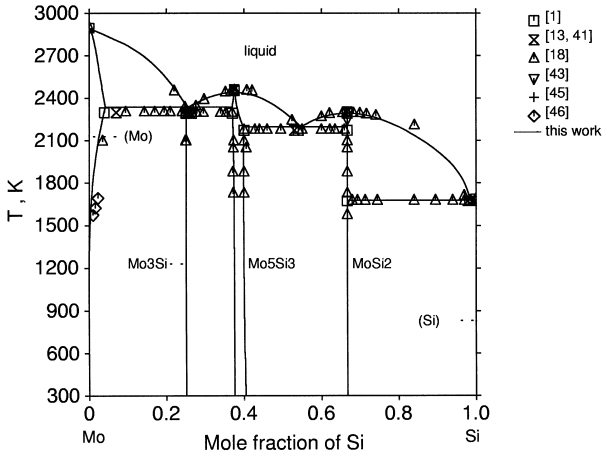

Fig. 8. The calculated phase diagram of the Mo–Si system compared with experimental data.

1873K given by [23, 24] differs greatly from the experimental results of [47], and also differ greatly from the results of [6] at 1823 K and [5, 29] at 1673 K. In reference [23], the connection of the $MoSi_2$-$C11_b + Mo_5Si_3 + MoSi_2$-C40 three-phase field with the ternary terminal end of the Mo_5Si_3 phase limits the range of Mo_5Si_3 compositions in the two-phase equilibrium region with C40 to a single point. This is impossible thermodynamically [27]. It is unlikely that the phase boundary will change so greatly with temperature. Based on the recent experimental results of [29,47], the wide composition range of the $Mo_5Si_3 + C40$ two phase field is apparently more reasonable.

The predicted liquidus projection is shown in Fig. 13. It predicts the following invariant reactions: liquid + $C11_b \rightarrow C40 + Mo_5Si_3$; liquid + $C40 + Mo_5Si_3 \rightarrow C54$; liquid + $C54 \rightarrow C40 + Al_8Mo_3$; liquid $\rightarrow Mo_5Si_3 + C54 + Al_8Mo_3$; liquid $\rightarrow Mo_5Si_3 + Mo_3(Al, Si) + Al_8Mo_3$; liquid + $Al_{63}Mo_{37} \rightarrow Mo_3(Al, Si) + Al_8Mo_3$; liquid + bcc $\rightarrow Al_{63}Mo_{37} + Mo_3(Al, Si)$; liquid + $Al_8Mo_3 \rightarrow C40 + Al_4Mo$.

The comparison between calculated enthalpies of formation of the hypothetical compounds $MoAl_2$-$C11_b$,

Table 4
Comparison between the calculated invariant equilibria and literature values in binary Mo–Si

Phase reaction	Composition of respective phases, x_{Si}			T (K)	Reference	
Liquid↔$Mo_3Si + Mo_5Si_3$	0.264			2293±20	[18]	Experimental
	0.26			2293±50	[13,41]	Experimental
	0.264	0.25	0.37	2293	[1]	
	0.256	0.25	0.370	2336.4	This work	Assessment
Liquid↔diamond + $MoSi_2$				~1683	[42]	Experimental
	0.985			1673±10	[18]	Experimental
	0.979			1673±10	[13,41]	Experimental
	0.983	1.0	0.667	1673	[1]	
	0.985	1.0	0.667	1680	This work	Assessment
Liquid↔$Mo_5Si_3 + MoSi_2$				2173±10	[43]	Experimental
	0.54			2173±20	[18]	Experimental
	0.53			2173±40	[13,41]	Experimental
				2163±31	[44]	Experimental
	0.54	0.40	0.667	2173	[1]	
	0.548	0.398	0.667	2196	This work	Assessment
bcc + liquid↔Mo_3Si		0.2746		2323	[45]	Experimental
		0.2572		2298±20	[18]	Experimental
	0.07	0.255		2298±40	[13,41]	Experimental
				2323±40	[44]	Experimental
	0.04	0.257	0.25	2298	[1]	
	0.042	0.253	0.25	2336.7	This work	Assessment
Mo_5Si_3↔liquid				2358±10	[43]	Experimental
		0.375		2453±20	[18]	Experimental
		0.375		2463±20	[13, 41]	Experimental
		0.375		2453	[1]	
		0.375		2441	This work	Assessment
$MoSi_2$↔liquid		0.667		2253±10	[43]	Experimental
				2293	[18]	Experimental
		0.667		2303±20	[13, 41]	Experimental
		0.667		2293	[1]	
		0.667		2293	This work	Assessment

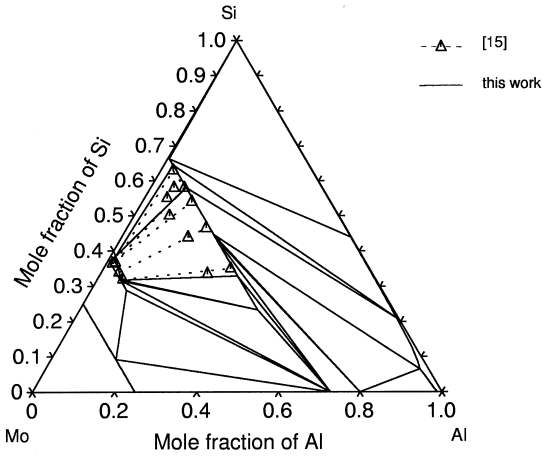

Fig. 9. The calculated isothermal section of the Al–Mo–Si system at 1273K compared with experimental data.

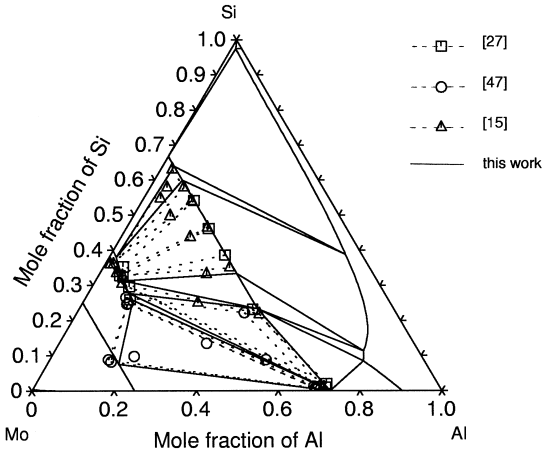

Fig. 10. The calculated isothermal section of the Al–Mo–Si system at 1673 K compared with experimental data.

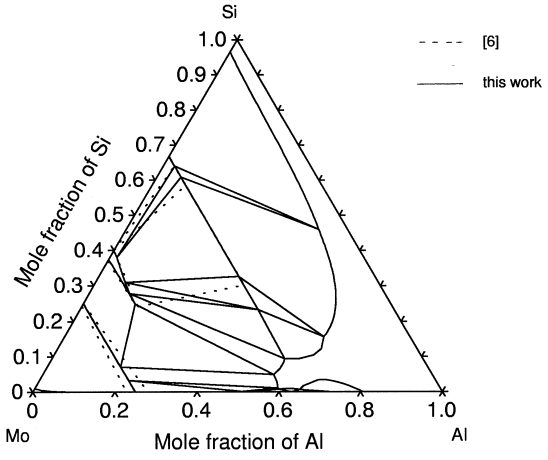

Fig. 11. The calculated isothermal section of the Al–Mo–Si system at 1823 K compared with experimental data.

$MoAl_2$-C40, Mo_5Al_3-D8 m and the Miedema's estimations are listed in Table 5.

The calculated enthalpy of transformation of $MoSi_2$ $C11_b$ to C40 at 0 K is listed is Table 6. The calculated value using first-principle theory at 0 K and the experimental value at 1110 K are also listed in Table 6. It is seen that the calculation agrees well with the the results of [21,34,35].

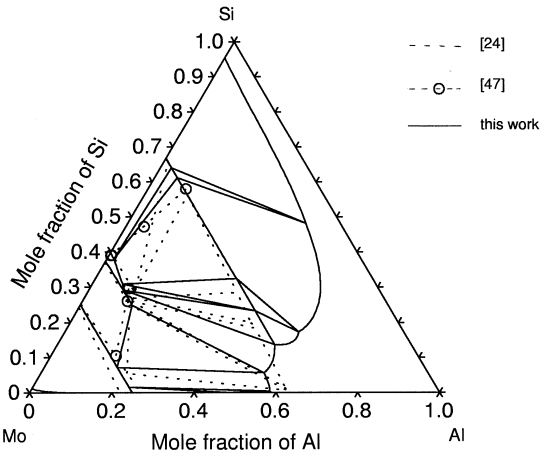

Fig. 12. The calculated isothermal section of the Al–Mo–Si system at 1873 K compared with experimental data.

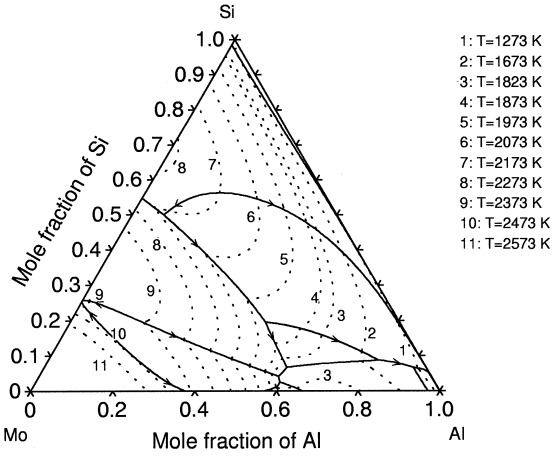

Fig. 13. The predicted liquidus projection to the composition triangle with isotherms (dotted line) superimposed.

Table 5
Calculated enthalpies of formation of hypothetical compounds

Hypothetical compounds	Enthalpy of formation, $\Delta^0 H_f$ [kJ/(mole of atom)]	
	Miedema's estimations [33]	This work
$MoAl_2$-$C11_b$	−20	−19.0
$MoAl_2$-C40	−20	−21.0
Mo_5Al_3-$D8_m$	−22	−7.3

Table 6
Transformation enthalpy of $MoSi_2$ $C11_b$ to C40

ΔH_{trans} [kJ/(mole of atoms)]	
This work	Literature values
−1.876	< −1.9 [34,35]; first principle calculation, 0 K −0.9±0.1 [21], experimental value, 1110 K

6. Summary

The Mo–Si and Al–Mo–Si systems have been thermodynamically assessed. The results are in good agreement with the experimental data. The high temperature phase equilibria involving the C40 and $C11_b$ $MoSi_2$ structures in the binary Mo–Si and ternary Al–Mo–Si systems have been clarified.

Acknowledgements

The authors would like to thank Professor J. Shen and Dr. K. Bai of the Beijing General Research Institute for Non-ferrous Metals for useful discussions. Partial financial support by the National Natural Science Foundation of China is acknowledged.

Appendix

A summary of thermodynamic parameters for the Al–Mo–Si ternary system is given below. Values are given in SI units and correspond to one mole of formula units. The L parameters refer to Redlich–Kister polynomials. The Gibbs energies of the pure elements are taken from [48] (parameters involving all three components are evaluated in the present work and the parameters which are not presented are zero).

$Al_{12}Mo$, sublattice model: $(Al)_{0.923}(Mo)_{0.077}$
$G_{Al:Mo} - 0.077\,{}^0G^{bcc}_{Mo} - 0.923\,{}^0G^{fcc}_{Al} = -10\,700 + 1.865T$
Al_5Mo, sublattice model: $(Al)_{0.833}(Mo)_{0.167}$
$G_{Al:Mo} - 0.167\,{}^0G^{bcc}_{Mo} - 0.833\,{}^0G^{fcc}_{Al} = -23\,000 + 4.381T$
Al_4Mo, sublattice model: $(Al)_{0.8}(Mo)_{0.2}$
$G_{Al:Mo} - 0.2\,{}^0G^{bcc}_{Mo} - 0.8\,{}^0G^{fcc}_{Al} = -26\,925 + 4.8T$
Al_8Mo_3, sublattice model: $(Al)_{0.727}(Mo)_{0.273}$
$G_{Al:Mo} - 0.273\,{}^0G^{bcc}_{Mo} - 0.727\,{}^0G^{fcc}_{Al} = -35\,470 + 7.12T$
$Al_{63}Mo_{37}$, sublattice model: $(Al)_{0.63}(Mo)_{0.37}$
$G_{Al:Mo} - 0.37\,{}^0G^{bcc}_{Mo} - 0.63\,{}^0G^{fcc}_{Al} = -13\,632 - 5.0\,T$
bcc_A2, sublattice model: (Al, Mo, Si) $(Va)_3$
${}^0L_{Al,Mo:Va} = -85\,000 + 20T$
${}^1L_{Al,Mo:Va} = -8000 - 5\,T$
${}^2L_{Al,Mo:Va} = -30\,000$
${}^0L_{Mo,Si:Va} = -60\,000 + 5T$
C40, sublattice model: $(Mo)_{0.333}(Al, Si)_{0.667}$
$G_{Mo:Si} - 0.333\,{}^0G^{bcc}_{Mo} - 0.667\,{}^0G^{dia}_{Si} = -43\,280 - 0.5\,T$
$G_{Mo:Al} - 0.333\,{}^0G^{bcc}_{Mo} - 0.667\,{}^0G^{fcc}_{Al} = -21\,000$
${}^0L_{Mo:Al,Si} = -21\,900 + 12T$
${}^1L_{Mo:Al,Si} = 2300$
C54, sublattice model: $(Mo)_{0.333}(Si)_{0.233}(Al)_{0.434}$
$G_{Mo:Si:Al} - 0.333\,{}^0G^{bcc}_{Mo} - 0.233\,{}^0G^{dia}_{Si} - 0.434\,{}^0G^{fcc}_{Al} = -33\,959.7 - 1.1\,T$
Diamond, sublattice model : (Al, Si)
${}^0L_{Al,Si} = 111\,417.7 - 46.1392\,T$
fcc_A1, sublattice model: (Al, Mo, Si) (Va)
${}^0L_{Al,Mo:Va} = -85\,300 + 20.4T$
${}^1L_{Al,Mo:Va} = -10\,000$
${}^0L_{Al,Si:Va} = -3423.91 - 0.09584\,T$
Liquid, sublattice model: (Al, Mo, Si)
${}^0L_{Al,Mo} = -110\,000 + 32T$
${}^1L_{Al,Mo} = -10\,000 + 6.6T$
${}^2L_{Al,Mo} = 5000$
${}^0L_{Al,Si} = -11\,655.93 - 0.92934\,T$
${}^1L_{Al,Si} = -2873.45 + 0.2945\,T$
${}^2L_{Al,Si} = 2520$
${}^0L_{Mo,Si} = -146\,600 + 16.5T$
${}^1L_{Mo,Si} = 7100 - 3T$
${}^2L_{Mo,Si} = 8000 + 12T$
Mo_3(Al,Si), sublattice model: $(Mo)_{0.75}(Al, Si)_{0.25}$
$G_{Mo:Al} - 0.75\,{}^0G^{bcc}_{Mo} - 0.25\,{}^0G^{fcc}_{Al} = -25\,250 + 3.0T$
$G_{Mo:Si} - 0.75\,{}^0G^{bcc}_{Mo} - 0.25\,{}^0G^{dia}_{Si} = -27\,900 - 0.28\,T$
${}^0L_{Mo:Al,Si} = -24\,650 + 8.75T$
$MoSi_2$_$C11_b$, sublattice model: $(Mo)_{0.333}(Al, Si)_{0.667}$
$G_{Mo:Si} - 0.333\,{}^0G^{bcc}_{Mo} - 0.667\,{}^0G^{dia}_{Si} = -45\,156 + 0.223T$
$G_{Mo:Al} - 0.333\,{}^0G^{bcc}_{Mo} - 0.667\,{}^0G^{fcc}_{Al} = -19\,000$
${}^0L_{Mo:Al,Si} = -4346 + 5\,T$
Mo_5Si_3, sublattice model: $(Mo, Si)_{0.625}(Si, Mo, Al)_{0.375}$
$G_{Mo:Si} - 0.625\,{}^0G^{bcc}_{Mo} - 0.375\,{}^0G^{dia}_{Si} = -38\,980 - 1.349\,T$
$G_{Si:Mo} - 0.625\,{}^0G^{dia}_{Si} - 0.375\,{}^0G^{bcc}_{Mo} = 58\,980 + 1.349T$
$G_{Mo:Mo} - {}^0G^{bcc}_{Mo} = 10\,000$
$G_{Si:Si} - {}^0G^{dia}_{Si} = 10\,000$
$G_{Mo:Al} - 0.625\,{}^0G^{bcc}_{Mo} - 0.375\,{}^0G^{fcc}_{Al} = -7300$
$G_{Si:Al} - 0.625\,{}^0G^{dia}_{Si} - 0.375\,{}^0G^{fcc}_{Al} = 10\,000$
${}^0L_{Mo,Si:Mo} = 10\,000$
${}^0L_{Mo:Mo,Si} = 20\,000$
${}^0L_{Si:Mo,Si} = 20\,000$
${}^0L_{Mo,Si:Si} = -68\,500 + 21.5T$
${}^0L_{Mo:AL,Si} = -20\,000$

References

[1] Gokhale AB, Abbaschian GJ. Journal of Phase Equilibria 1991;12(4):493–8.
[2] Samsonov GV, Vinitskii IM. Handbook of refractory materials. New York: IFI Plenum, 1980.
[3] Costa e Silva A, Kaufman MJ. Scripta Metallurgica et Materialia 1993;29:1141–5.
[4] Deevi SC, Deevi S. Scripta Metallurgica et Materialia 1995;33(3):415–20.
[5] Kodash VU, Kisly PS, Shemet VJ. High Temperature Science 1990;29:143–52.
[6] Yanagihara K, Maruyama T, Nagata K. Materials Transactions, JIM 1993;34(12):1200–6.
[7] Stergion A, Tsakiropoulos. Materials Research Society Symposium Proceedings 1995;364:911–6.

[8] Ross EN, Eason PD, Kaufman MJ. Processing and Fabrication of Advanced Materials V. In: Proceedings of TMS Annual Meetings, 1996. p. 347–360.
[9] Smialek JL, Nesbitt JA, Brindley, Brady MP, Doychak J, Richardson RM, Hull DR. In: Materials Research Society Symposium. Materials Research Society, 1995.
[10] Saunders N. Journal of Phase Equilibria 1997;18(4):370–8.
[11] Chakraborti N, Lukas HL. Calphad 1992;16(1):79.
[12] Kaufman L. Database of Thermo-Calc software. Stockholm: Royal Institute of Technology, 1997.
[13] Brewer L, Lamoreaux LH. In: Brewer L, editor. Atomic Energy Review, (special issue no. 7) Vienna, 1980. p. 320.
[14] Vahlas C, Chevalier PY, Blanquet E. Calphad 1989;13(3):273–92.
[15] Costa e Silva A. Synthesis of molybdenum disilicide composites using in-situ reactions, PhD. dissertation, University of Florida, Gainesville, FL, 1994.
[16] Bai K, Shen J. CALPHAD XXVIII, Grenoble, France, 2–7 May 1999.
[17] Svechnikov VN, Kocherzhinskii YuA, Yupko LM. Soviet Physics — Doklady 1969;13(10):1072–3.
[18] Svechnikov VN, Kocherzhinskii YuA, Yupko LM. In: Ageev NV, editor. Diagrammy Sostoyaniya Metal Sist. Nauka. Moscow, 1971. p. 116–9.
[19] Svechnikov VN, Kocherzhinskii YuA, Yupko LM. Dokl Akad Nauk Ukrain RSR, Sevchnikov & Kocherzhinsky 1972;6A:566–70.
[20] Frankwicz PS, Perepezko JH. Mat Res Soc Symp Proc 1991;21:169–74.
[21] Frankwicz PS, Perepezko JH. Materials Science and Engineering A246:199–206
[22] Boettinger WJ, Perepezko JH, Frankwicz PS. Materials Science and Engineering A155:33–44
[23] Brukl C, Nowotny H, Benesovsky F. Monatsh Chem 1961;92:967–80.
[24] Guzei LS. Aluminum–Molybdenum–Silicon. In: Petsow G, Effenberg G, editors. Ternary alloys — a comprehensive compendium of evaluated constitutional data and phase diagrams, vol. 7. Weinheim (Germany): VCH Verkgsgesellschaft, 1993. p. 225–8.
[25] Massalski TB, editor. Binary alloy phase diagrams. Metals Park (OH): ASM International, 1986.
[26] Maruyama T, Bi XF, Nagata K. In: High temperature corrosion of advanced materials and protective coatings. Saito Y, Onay B, Maruyama T, editors. Elsevier Science Publishers, 1992. p. 291–9.
[27] Eason PD, Jolly KL, Kaufman MJ. Reassessment of the Mo–Si–Al ternary isotherm at 1400°C, 22nd Annual Conference on Composites, Advanced Ceramics, Materials and Structures, FL, USA, January 1998. p. 437–44.
[28] Sundman B. Ågren J J Phys Chem Solids 1981;42:297–301.
[29] Saunders N, Miodownik AP. CALPHAD (calculation of phase diagrams): a comprehensive guide. Pergamon, 1998.
[30] Redlich O, Kister AT. Ind Eng Chem 1948;40:345.
[31] Sundman B, Jansson B, Andersson JO. Calphad 1985;9:153.
[32] Arpaci E, Frohberg MG. Z Metallkunde 1985;76:440–4.
[33] Boer FR, Boom R, Mattens WCM, Miedema AR, Niessen AK. Cohesion in metals — transition metal alloys. V: North-Holland: Elsevier Science Publishers B, 1989.
[34] Carlsson AE, Meschter PJ. J Mater Res 1991;7:1512.
[35] Matthesis LF. Phys Rev B 1992;45:3252.
[36] Hultgren R, Desai PD, Hawkins DT, Gleiser M, Kelley KK. Selected values of the thermodynamic properties of binary alloys. Metals Park (OH): ASM International, 1973. p. 1158–63
[37] Chart TG. Metal Science 1974;8:344–8.
[38] Chart TG. High Temperatures–High Pressures 1973;5:241–52.
[39] Barin I, Sauert F, Schultze-Rhonhof E, Sheng W.S. Thermochemical data of pure substances. Weinheim (Germany): VCH Verlagesellchaft mbH, 1989:931–3.
[40] Miodownik AP. In: Kùbaschewski O, editor. Metallurgical Chemistry. London, HMSO, 1972. p. 233.
[41] Moffat WG. The handbook of binary phase diagrams. General Electric Company, 1981.
[42] Hansen M, Anderko K. Constitution of binary alloys. McGraw-Hill, 1958.
[43] Cherniack GB, Elliot AG. Journal of The American Ceramic Society 1964;47(3):136–41.
[44] Zotov YuP, Kroshkina NN, Bukharin VE. Neorgan Mater 1980; 16(5):842–5.
[45] Kieffer R, Cerwenka E. Z Metallkunde 1952;43:101–5.
[46] Ham JL. Trans ASME 1951;73:723–31.
[47] Arvanitis A. PhD research in progress, University of Surrey, 2000.
[48] Dinsdale AT. Calphad 1991;15:317.